Journal of the Korean Ceramic Society
Vol. 42, No. 2, pp. 140~144, 2005.

Communication

Microstructures and Mechanical Properties of Pressureless and Spark Plasma Sintered ZrO_2(3 mol%Y_2O_3) Bodies

Na-Young Shin, Jae-Kil Han, Hae-Hyoung Lee,* and Byong-Taek Lee†

School of Advanced Materials Engineering, Kongju National University, Kongju City 314-701, Korea
**Department of Dental Biomaterials, School of Dentistry, Dankook University, Cheonan City 330-714, Korea*
(Received September 14, 2004; Accepted December 6, 2004)

ABSTRACT

The microstructures and mechanical properties of Tetragonal Zirconia Polycrystals (TZP) sintered bodies, which made by pressureless and spark plasma sintering techniques, were investigated using XRD, SEM, and TEM techniques. In the spark plasma sintered samples, the TZP grains were equiaxed type including many sub-grain boundaries regardless of sintering conditions. The biaxial strength of TZP having an average of 80 nm grains in diameter was high in value with 1025 MPa, but fracture toughness showed a low value due to the absence of a fracture toughening mechanism such as transformation toughening. In the Pressureless Sintered (PLSed) samples, the grain size of TZP was strongly dependent on the sintering temperature; i.e., it gradually increased as the sintering temperature increased. The value of fracture toughness increased as the grain size increased by the stress-induced phase transformation and some crack deflection.

Key words : Nano crystalline ZrO_2, Spark plasma sintering, Pressureless sintering, Mechanical property, Microstructure

1. Introduction

Tetragonal Zirconia Polycrystalline (TZP) ceramic is well known as a typical bioceramic because it is non-toxic, non carcinogenic and non allergenic in a human body.[1,2] The good biocompatibility leads to the medical applications such as dental materials,[3,4] bone fixation,[5,6] and hip prostheses.[7] Furthermore, TZP has been widely used in industrial materials[8,9] such as metal forming dies and chemical components and as a toughening agent in the Al_2O_3[10-14] and Si_3N_4[15] ceramic matrix systems. This is basically caused by the reduction of crack propagation energy by the stress-induced martensite phase transformation; i.e., when some cracks are propagated into the sintered body, the TZP grains around the cracks are transformed to a monoclinic phase which is accompanied by some volume change and twins as internal defects. It is well-known that the grain size of TZP with sub-micron-sized grains has a strong effect on the phase transformation temperature of TZP.[16]

Recently, nano ceramics having nano-crystalline grains in the body has been actively investigated using nano ceramic powders. For the production of a nano crystalline sintered body, the Spark Plasma Sintering (SPS) technique[17,18] has been widely used because it is an easy, fast heating process and can be sintered at a lower temperature than that of conventional sintering techniques. There are a few advantages in using nano powders in ceramic engineering, such as the possibility of low-temperature sintering due to its high specific surface area, the application of small sized components for the MEMS, and the formation of super-plastic. However, there were no detailed reports on the comparison of microstructures and material properties of TZP with nano and submicron grain size. Thus, in this work, the grain size effect on the mechanical properties of TZP sintered bodies having nano and submicron sized grains was investigated.

†Corresponding author : Byong-Taek Lee
E-mail : lbt@kongju.ac.kr
Tel : +82-41-850-8677 Fax : +82-41-850-2939

2. Experimental Procedures

Using the uniaxial lever press under 10 kg/mm^2, the ZrO_2 (3 mol%Y_2O_3) powder (Tosoh, TZ-3YB) were compacted into a disk shape of 20 mm in diameter. To obtain the various submicron sized grains in the pressureless sintered (PLSed) body, the PLS was performed at temperatures ranging from 1450°C to 1650°C for 2 h. To obtain the nano crystalline sintered body, some portion of the ZrO_2 powder was directly sintered by the SPS process using a graphite mold at 1000°C for 5 min. The detailed sintering conditions used in this present work are shown in Fig. 1. The morphology and phase analysis of ZrO_2 powders and their sintered bodies made at each condition were identified by F-SEM (JSM, JEOL, Japan) and XRD (DMAX250, Rigaku) techniques, respectively. The image analyzer was used to measure the average grain size of sintered bodies. Using TEM (JEM 2010, JEOL), the detailed internal microstructures of raw ZrO_2 powders and sintered bodies were examined. The Vick-

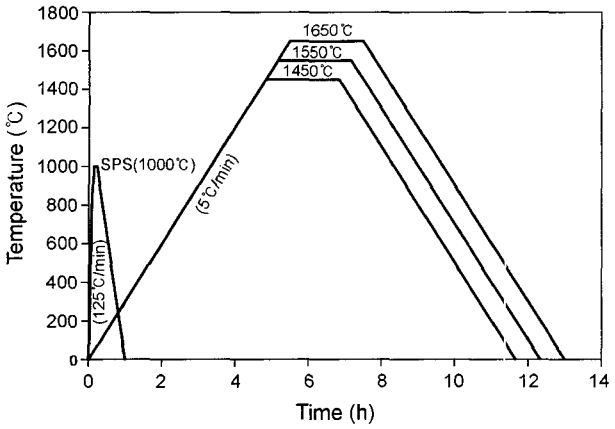

Fig. 1. Schematic sintering schedule for making the sintered bodies.

ers hardness (HV-112, Akashi) was measured by indenting with a load of 500 g. The biaxial strength was determined by a piston-on-3-ball technique, which was based on the ASTM F394-78 for dental materials. Disk specimens supported on three ball bearings (3.2 mm in diameter) were tested at a constant loading rate of 1.2 kN/min. The fracture toughness (K_{1C}) was calculated by the indentation method using a load of 20 Kg.[19] The fracture surfaces which were made by a biaxial test were observed by SEM.

3. Results and Discussion

Fig. 2(a) shows TEM image of ZrO_2 powders synthesized one in this work. The average size of the ZrO_2 particles having an equiaxed shape was about 70 nm in diameter and they were agglomerated with several particles. In an enlarged HRTEM image (b), some lattice distortion was observed in the internal. It seems to be caused by the solid solution due to the doping of 3 mol%Y_2O_3. However, the internal defects such as twins and dislocations frequently observed in m- ZrO_2 particles were not observed.[12]

Fig. 3 shows SEM images of thermal-etched ZrO_2 bodies depending on the sintering temperatures. In the SPSed sample (a), the average grain size was about 80 nm and it had a comparatively uniform size. The average grain sizes in the PLSed bodies sintered at 1450°C (b), 1550°C (c), and 1650°C (d) were 260 nm, 490 nm, and 770 nm, respectively; i.e., the grain size gradually increased as the sintering temperature increased. There are large, equiaxed-grains of

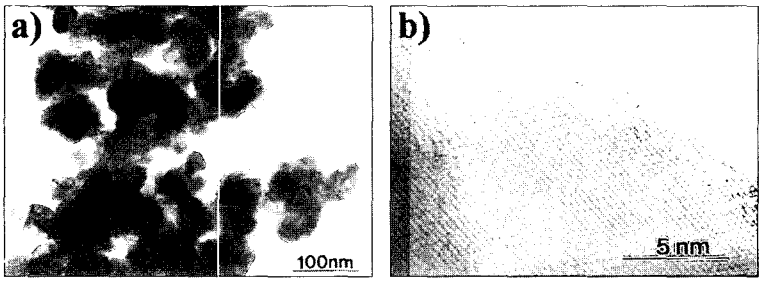

Fig. 2. TEM (a) and HRTEM (b) images of TZP nano powder.

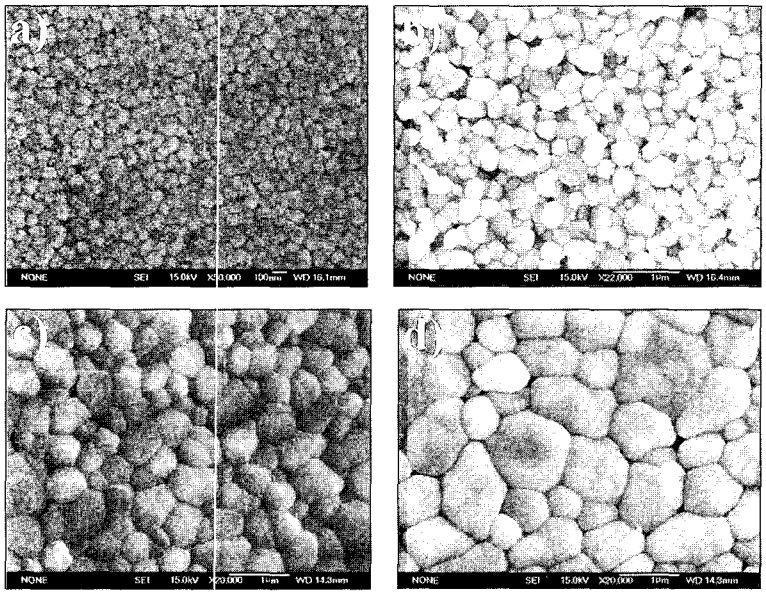

Fig. 3. Thermal etched SEM images of TZP sintered bodies made by (a) SPS at 1000°C, (b) PLS at 1450°C, (c) 1550°C, and (d) 1650°C.

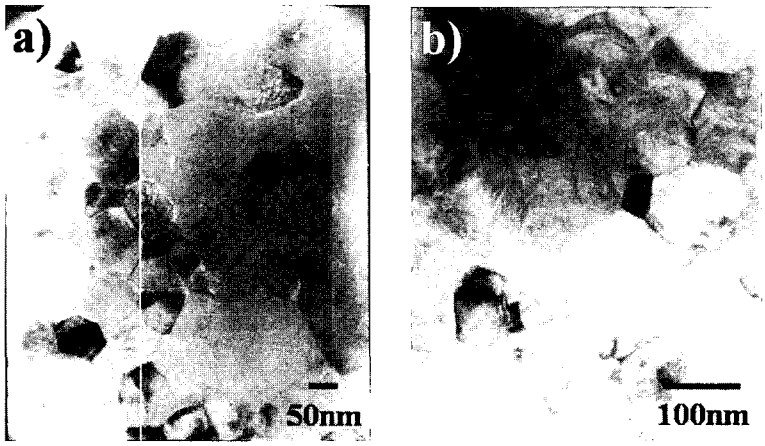

Fig. 4. TEM images showing internal microstructure of (a) SPS and (b) PLS at 1450°C.

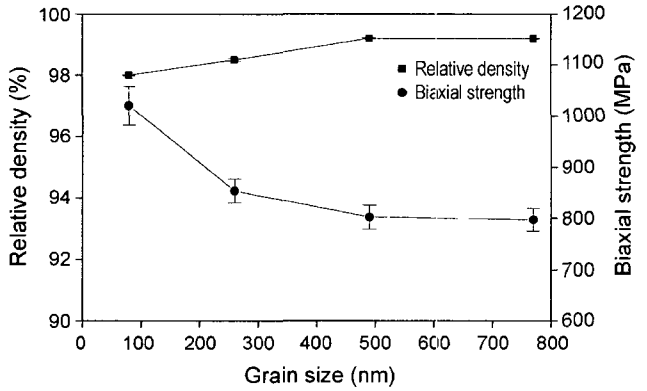

Fig. 5. Relative density and biaxial strength of TZP sintered bodies with the grain size.

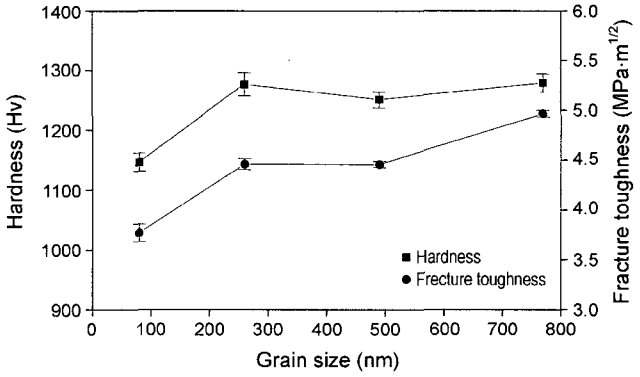

Fig. 6. Hardness and fracture toughness of TZP sintered bodies with the grain size.

about 1200 nm although small grains are also present, as shown in Fig. 3(d).

Fig. 4(a) and (b) show TEM images of SPSed and PLSed (1450°C) samples, respectively. Regardless of sintering conditions, the grain shape was equiaxed and included strain field contrast. This is due to the existence of several subboundaries in most ZrO_2 grains although the intensity of the PLSed sample was higher than that of the SPSed sample.

Fig. 5 shows the values of relative density and biaxial strength depending on the average grain size. In spite of the comparatively low temperature and short duration time, the relative density of the SPSed sample having 80 nm sized grains was comparatively high at 98.1%. In the PLSed sample, the relative density gradually increased as the grain size increased due to the increasing of sintering temperature, and then it become saturated at about 99.2% in the sample having 490 nm sized grain and over. On the other hand, the biaxial strength of the SPSed sample having 80 nm sized grain was a maximum value of 1025 MPa. But the biaxial strength of the PLSed samples decreased as the grain size increased; i.e., as the sintering temperature increased.

Fig. 6 shows the values of Vickers hardness and fracture toughness with average grain sizes. In the PLSed samples having larger than 260 nm sized grain, their hardness values were around 1270 Hv without any remarkabe difference regardless of the sintering temperature. However, in the SPSed sample having 80 nm sized grain, the value was low with 1150 Hv, caused by the low value of relative density. An interesting result is that the value of fracture toughness in the SPSed sample having 80 nm sized grain showed a minimum value with 3.7 MPa · $m^{1/2}$. On the other hand, fracture toughness increased as the average grain size increase and then showed a maximum value 5.0 MPa · $m^{1/2}$ in the PLSed sample having 770 nm sized grains that was sintered at 1650°C.

Fig. 7 shows the SEM fracture surfaces made by a biaxial test. In the low magnification image of the SPSed sample, the fracture surface was seen with very fine contrast because it was constructed with nano-crystalline structure as shown in Fig. 3(a). From the enlarged image in Fig. 7(a), the main fracture mode was an intergranular type having a rough and sharp surface. In the PLSed samples sintered at 1450°C, the fracture mode was a mixed fracture type with intergranular and transgranular modes, respectively, showing sharp and flat surfaces. As the sintering temperature increased, the portion of transgranular mode decreased.

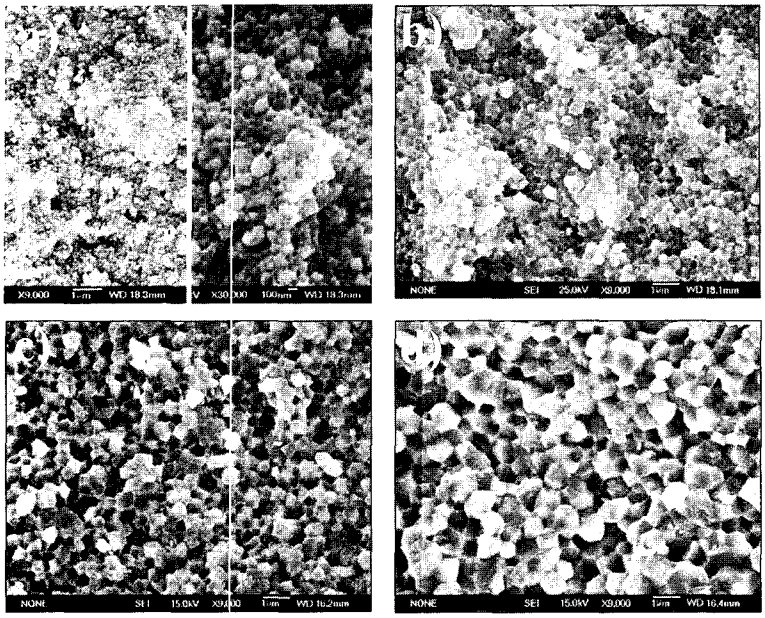

Fig. 7. SEM fracture surfaces of TZP sintered bodies made by (a) SPS at 1000°C, (b) PLS at 1450°C, (c) 1550°C, and (d) 1650°C.

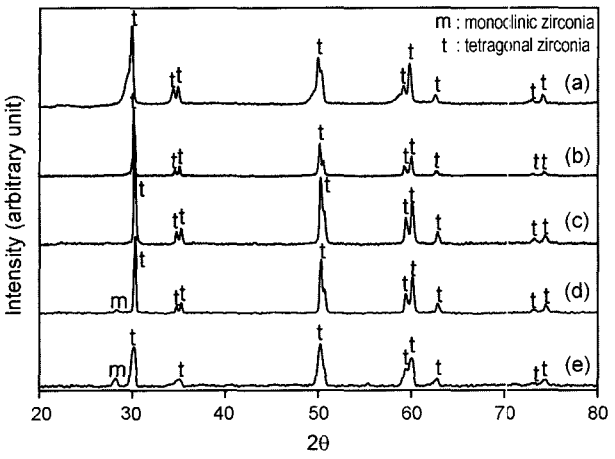

Fig. 8. XRD profiles of TZP sintered bodies and fracture surfaces. (a) SPS (before fracture), (b) PLS at 1450°C (before fracture), (c) SPS (after fracture), (d) PLS at 1450°C (after fracture), and (e) PLS at 1650°C (after fracture).

For the comparison of the change of crystal structure in the samples having as-received and as-fractured samples, the XRD profiles were obtained from each of the samples. As seen in Fig. 8(a) and (b), the SPSed and PLSed bodies were comprised of just the t-ZrO_2 crystalline phase. On the other hand, in the fracture surface of the SPSed body, there was no change of crystal structure as can be seen in Fig. 8 (c). In the fractured samples sintered at 1450°C and 1650°C, although the main peaks were t-ZrO_2 phase, a monoclinic peak was also detected with a weak intensity due to the stress-induced phase transformation. An important observation is that the intensity of the monolithic phase increased as the sintering temperature increased (or as the grain size increase) as shown in Fig. 8(d) and (e). This result is consistent with the previous results having large grains with on a submicron- and micro-scale.[16]

In recent years, many works on TZP sintering using nano-technology have many week been increasingly conducted, and the SPS process stands in the center of investigation. However, it is rare to find a clear report on the mechanical properties of nano-crystalline TZP sintered body, compared with that in submicron or micron grades. It is known that the use of the SPS process gives rise to a suppression of grain growth during sintering, resulting in an effective way of nano-microstructure control.[20] The TZP having nano-grains, however, showed relatively lower fracture toughness than that having submicron or micron sized grains. This is attributed to the fact that the stress induced phase transformation does not occur during sintering, due to grain refinement. The weak crack deflection is another reason because the crack deflection in the PLSed samples, which have coarse grains, generally happens more effectively. Taken as a whole, there is a limit to enhancing the fracture toughness of monolithic SPSed TZP using nano-powders. Thus, it is necessary to newly design the composites using the different materials properties of nano-sized metallic powders such as their thermal expansion coefficient, elastic modulus and lattice distance, etc. The biaxial strength of the TZP decreased as the grain size increased as shown in Fig. 5.

4. Conclusions

From the study on the effect of grain size on the material properties of TZP sintered bodies having nano and submicron sized grains, the following results were obtained. Nano crystalline TZP sintered bodies having an average diameter of 80 nm were obtained using the SPS process. In the PLSed samples sintered at 1450°C, 1550°C, and 1650°C, their grain

sizes were about 250 nm, 470 nm, and 770 nm, respectively. The grain shape of the TZP samples was of the equiaxed type including many sub-grain boundaries regardless of the sintering conditions. In the SPSed sample having 80 nm sized grain, the biaxial strength was a maximum value of 1025 MPa, but the fracture toughness showed a low value due to the absence of phase transformation toughening. However, in the PLSed sample, the value of fracture toughness increased as the grain size increased due to the stress-induced phase transformation.

Acknowledgement

This work was supported by NRL research program of the Korean Ministry of Science and Technology.

REFERENCES

1. C. Fernandez, E. Verne, J. Vogel, and G. Carl, "Optimisation of the Synthesis of Glass-Ceramic Matrix Biocomposites by the Response Surface Methodology," *J. Eur. Ceram. Soc.*, **23** [7] 1031-38 (2003).
2. A. Marti, "Inert Bioceramics(Al_2O_3, ZrO_2) for Medical Application," *Int. J. Care Injured*, **31** S-D33-36 (2000).
3. V. Stanic, N. N. Aldini, and M. Fini, "Osteointegration of Bioactive Glass-Coated Zirconia in Healthy Bone : An in vivo Evaluation," *Biomater*, **23** [18] 3833-41 (2002).
4. R. Janda, J. Roulet, M. Wulf, and H. Tiller, "A New Adhesive Technology for All-Ceramics," *Dent. Mater.*, **19** [6] 567-73 (2003).
5. C. Piconi, W. Burger, and H. Richter, "Y-TZP Ceramics for Artificial Joint Replacements," *Biomater*, **9** 1489-94 (1998).
6. P. Torricelli, E. Verne, and C. V. Brovarone, "Biological Glass Coating on Ceramic Materials : In vitro Evaluation Using Primary Osteoblast Cultures from Healthy and Osteopenic Rat Bone," *Biomater*, **22** [18] 2535-43 (2001).
7. L. Yin, S. Jahanmir, and L. K. Ives, "Abrasive Machining of Porcelain and Zirconia with a Dental Handpiece," *Wear*, **255** 975-89 (2003).
8. C. Z. Huang, B. Zhang, and L. He, "A Study on the Development of a Composite Ceramic Tool ZrO_2/(W,Ti)C and Its Cutting Performance," *J. Mater. Proc. Tech.*, **129** 349-53 (2002).
9. T. Sornakumar, R. Krishnamurthy, and C. V. Gokularathnam, "Machining Performance of Phase Transformation Toughened Alumina and Partially Stabilised Zirconia Composite Cutting Tools," *J. Eur. Ceram. Soc.*, **12** [6] 455-60 (1993).
10. B. Smuk, M. Szutkowska, and J. Walter, "Alumina Ceramics with Partially Stabilized Zirconia for Cutting Tools," *Mater. Proc. Tech.*, **133** 195-98 (2003).
11. B. T. Lee, K. Hiraga, D. Shindo, and A. Nishiyama, "Microstructure of Pressureless-Sintered Al_2O_3-24 Vol-Percent ZrO_2 Composite Studied by High-Resolution Electron-Microscopy," *J. Mater. Sci.*, **29** [4] 959-64 (1994).
12. B. T. Lee, A. Nishiyama, and K. Hiraga, "Micro-Indentation Fracture Behavior of Al_2O_3-24 vol% ZrO_2 Composite Studied by High-Resolution Electron Microscopy," *Mater. Trans., JIM.*, **34** 682-86 (1993).
13. B. T. Lee and K. Hiraga, "Crack-Propagation and Deformation-Behavior of Al_2O_3-24 vol-Percent ZrO_2 Composite Studied by Transmission Electron-Microscopy," *J. Mater. Res.*, **9** [5] 1199-207 (1994).
14. B. T. Lee and K. Hiraga, "Stress-Induced Phase Transformation of ZrO_2 in ZrO_2 (3 mol%Y_2O_3)-25 vol%Al_2O_3 Composite Studied by Transmission Electron Microscopy," *Scrip. Mater.*, **38** [7] 1101-07 (1998).
15. B. T. Lee, T. Koyama, A. Nishiyama, and K. Hiraga, "Microstructure and Fracture Characteristic of Si_3N_4-ZrO_2(MgO) Ceramic Composite Studied by Transmission Electron Microscopy," *Scrip. Meta. et Mater.*, **32** [7] 1073-77 (1995).
16. P. F. Becher and M. V. Swain, "Grain-Size-Dependent Transformation Behavior in Polycrystalline Tetragonal Zirconia," *J. Am. Ceram. Soc.*, **75** [3] 493-97 (1992).
17. X. J. Chen, K. A. Chan, S. H. Chan, and L. G. Yu, "Preparation Yttria-Stabilized Zirconia Electrolyte by Spark-Plasma Sintering," *Mater. Sci. and Eng. A*, **341** 43-9 (2003).
18. M. Nygren and Z. Shen, "On the Preparation of Bio-, Nano-, and Structural Ceramics and Composites by Spark Plasma Sintering," *Sol. Stat. Sci.*, **5** [1] 125-31 (2003).
19. J. Lu, L. Gao, and J. Sun, "Effect of Nickel Content on the Sintering Behavior, Mechanical, and Dielectric Properties of Al_2O_3/Ni Composites from Coated Powders," *Mater. Sci. Eng. A*, **293** 223-28 (2000).
20. K. A. Khor, L. G. Yu, S. H. Chan, and X. J. Chen, "Densification of Plasma Sprayed YSZ Electrolytes by Spark Plasma Sintering (SPS)," *J. Am. Ceram. Soc.*, **23** 1855-63 (2003).